JOURNAL OF Applied Polymer SCIENCE

In Situ WAXS/SAXS Structural Evolution Study During Uniaxial Stretching of Poly(ethylene therephthalate) Nanocomposites in Solid State: Poly(ethylene therephthalate)/Montmorillonite Nanocomposites

Lyudmil V. Todorov, Carla I. Martins, Júlio C. Viana
Institute for Polymers and Composites/I3N, Department of Polymer Engineering, University of Minho, 4800-058 Guimarães, Portugal
Correspondence to: J. C. Viana (E-mail: jcv@dep.uminho.pt)

ABSTRACT: This work investigates the solid state uniaxial stretching of neat polyethylene therephthalate, PET, and its montmorillonite, MMT, nanocomposites (0.3 wt % of MMT particles with different initial agglomerate sizes) showing intercalated and tactoid morphologies, followed by *in situ* WAXS and SAXS experiments under an X-ray synchrotron source. The distinct nanocomposite morphologies were assessed by WAXS and transmission electron microscopy. The *in situ* WAXS experiments during stretching evaluated the evolution of phase's mass fractions and the average level of molecular orientation upon uniaxial deformation, and the *in situ* SAXS experiments assessed the evolution of craze-like structures and void sizes. Multiscale structure evolution models are proposed and compared for neat PET and its nanocomposites. Main global mechanisms are identical although with distinct evolutions of phase mass fractions. Also craze-like/voids structures evolve with distinct sizes. Intercalated MMT morphology induces an earlier formation of periodical mesophase, a retarded widening of craze-like structures and the smallest void sizes.© 2012 Wiley Periodicals, Inc. J. Appl. Polym. Sci. 000: 000–000, 2012

KEYWORDS: X-ray; phase behavior; clay; morphology

Received 31 May 2012; accepted 19 July 2012; published online
DOI: 10.1002/app.38368

INTRODUCTION

Within the last decade it has been clearly recognized that inorganic nanoscale reinforcements have become an attractive mean of improving the properties and stability of polymers with very low incorporation of nanoparticles (typically <5 wt %). This led to a new class of composites, the polymer nanocomposites, PNCs.[1] Because of the high surface-to-volume ratio of the nanofillers, innumerous interactions are developed with the polymer macromolecular chains, that can operate as structure and morphology directors and may also introduce new energy dissipation mechanisms.[2]

Poly(ethylene therephthalate), PET, nanocomposites reinforced with layered silicates, particularly montmorillonite, MMT, became an important alternative for neat PET for packaging applications with improved mechanical, barrier, and thermal properties. The nanocomposite properties depend on the delamination of MMT nanoparticles into the polymer matrix. These can be (i) tactoid—unseparated MMTs layers, (ii) intercalated—regularly alternating MMT's and polymer layers with a repeating distance of a few nanometers, and (iii) exfoliated—irregularly delaminated and well-dispersed lamellas of MMT.[3] These distinct structures play a key role in the enhancement of the PNC properties. Normally, exfoliated PNCs have superior mechanical properties than intercalated nanocomposites.[4–8] To delaminate and disperse MMT in the PET matrix it is necessary to introduce organic modifiers (organo modified MMT, oMMT). This process changes the MMT's substrate from hydrophilic to hydrophobic for better insertion of hydrophobic PET molecular chains into the gallery between the layers of MMT. In this case, improved delamination and dispersion of MMT in the PET matrix is achieved.

The incorporation of MMT nanofillers in the PET polymer matrix have been made via various methods, namely: (i) *in situ* polymerization,[9–19] (ii) solvent assisted blending,[9–11] and direct melt blending.[12–23] Melt blending techniques are recognized as an attractive pathway to produce PNC in a commercial scale, due to: (i) the fast dispersion of nanofillers in the melt, (ii) the availability of melt compounding capacities, and (iii) the environmentally friendly preparation.1 A variety of blending apparatus were used for compounding of PET with MMT nanoparticles, specifically: (i) corotating twin-screw extruder,[12,14,15,21,22,24,25] (ii) corotating twin-screw micro extruder,[26,27] (iii) contrarotating extruder,[16] (iv) extrusion and subsequent injection moulding,[17,18,23] and direct injection molding.[17,23] However, the main limitations

of melt blending methods are the delamination of MMT's layers into the polymer matrix and the thermal decomposition of the organic surfactants.[21] Successful melt dispersion requires the presence of strong interactions between the inorganic nanofillers and the macromolecules, an appropriate stress field and an enough residence time. In the literature many works report about PET/MMT nanocomposites with enhanced tensile mechanical properties, produced via melt blending, namely: (i) higher modulus,[12,15–18,25] (ii) higher strength,[12,14,18] and (iii) higher deformability.[14]

Until now, research efforts have been devoted to the characterization of the deformation mechanism of PNCs with MMT during uniaxial stretching, as a function of the degree of delamination of MMT. Kim et al.[28,29] identified that the main deformation mechanism is through microvoid formation inside tactoids or intercalated MMT particles. The originated void size is directly related to the MMTs morphology, thus intercalated state resulting in smaller voids than the tactoid one.[28] Three possible modes of deformation were identified depending on MMT's particles position toward the stretching direction: (i) perpendicular (splitting) were deformation initiates at the middle region of the stacked MMT's particles (tactoid) or platelets splitting takes place in the middle of intercalated MMT particle, (ii) at a certain angle (opening)—opening of bundles of the stacked particles (tactoids) or bundles of the intercalated MMT layers occurs during the deformation process, and (iii) parallel (slipping)—slipping bundles of the stacked MMT's particles in case of tactoid morphology and sliding of pallets of MMT particles for intercalated one. Recent works based on *in situ* SAXS investigation of PET nanocomposites with carbon nanotubes[30,31] and carbon black[31] evidenced as well matrix craze-like formation with voiding during uniaxial stretching in the solid state. However, the incorporation of the inorganic nanoparticles retarded the growth and failure of the crazes during deformation.[30,31]

To improve and control the ultimate mechanical properties for a wide range of applications and, in particular to optimize the stiffness/toughness balance, a better understanding of the interrelationship between the MMT morphologies and structure evolution during the mechanical deformation processes is required. In this context, this work aims at understanding the effect of MMT nanofillers incorporation within a PET matrix on the structure evolution and deformation mechanism taking place during uniaxial stretching in the solid state.

EXPERIMENTAL

Materials

In this work the following materials were used: Poly(ethylene terephthalate), PET, with intrinsic viscosity of 0.74 ± 0.02 dL g^{-1} (bottle grade), provided by Tergal Fibers S.A., France. Nanoparticles: organo-modified (with stearylbenzyldimethylammonium chloride) MMT, oMMT, with different powder agglomerates size, namely: (i) Nanofil®32, called MMT32 and (ii) Nanofil®2, called MMT2. These materials were supplied by Süd-Chemie AG, Germany. Their specifications are given in Table I.

Table I. Nanoparticles Specifications (According to Supplier Data)

Nanoparticles	$D_{aggl.}$ (μm)	$d_{(001)}$ (nm)	UTBD (g L^{-1})	Surfactant
MMT32	30–80	1.8	350	long chain hydrocarbon/ benzyl group
MMT2	8–12	1.8	150	long chain hydrocarbon/ benzyl group

$D_{aggl.}$—powder agglomerates main average diameter, $d_{(001)}$—interlayer distance of basal plane (001), UTBD—untamped bulk density.

Sample Preparation

Samples used in this work where produced via direct melt blending of PET with 0.3 wt % of MMT, using an asymmetric batch minimixer according to the experimental procedure described in our previous work [44] After blending, compression molded samples were prepared and cooled down very rapidly on a water container at 5°C to obtain amorphous PET plaques. These plaques were then cut with a curved axisymmetric shape and used for the *in situ* WAXD and SAXD simultaneous to the uniaxial tensile testes (sample dimensions—length 35 mm, minimum cross-section 14 × 0.3 mm^2 and curvature radius of 10.4 mm. The grip distance was of 14 mm).

Nanocomposites Characterization

Off-line Wide Angle X-ray Scattering, WAXS. WAXS was performed on a AXS NanoStar Bruker equipment working with Cu Kα radiation ($\lambda = 0.154$ nm). The sample-to-detector distance was 99 mm and 2D WAXS patterns were acquired with a 2D HI-STAR Area Detector with accumulation time of 600 s. The WAXS patterns were analyzed in the range of $2\theta = 1.6°–10°$, to study the delamination of the MMTs.

Transmission Electron Microscopy, TEM. Particles agglomerates sizes where obtained using TEM micrographs taken from ultramicrotome cuts of ~60 nm of thickness, made through the thickness of the compression molded samples. For that a JEOL JEM 1010, at a voltage of 100 kV was used. Three micrographs per nanocomposite were used for particles agglomerates measurements from randomly transversal cuts. MMT's particles incorporated into PET nanocomposites were assumed to be elliptical. The average agglomerate (cluster of intercalated particles or tactoids) diameter, $D_{av,}$ was calculated by:

$$D_{av} = \frac{\sum_{i=1}^{n} [(d_1 + d_2)_i/2]}{n} \quad (1)$$

where d_1 and d_2 are the main diameters of each agglomerate and n is the number agglomerates considered (at least five TEM particle measurements were considered).

Simultaneous Deformation and *In Situ* Synchrotron Characterization

Uniaxial continuous stretching in the solid state (at 23°C) and *in situ* WAXS and SAXS characterization were performed simultaneously. WAXS and SAXS were carried out under synchrotron radiation (Ge (111) and $\lambda = 0.15$ nm) at HASYLAB, DESY,

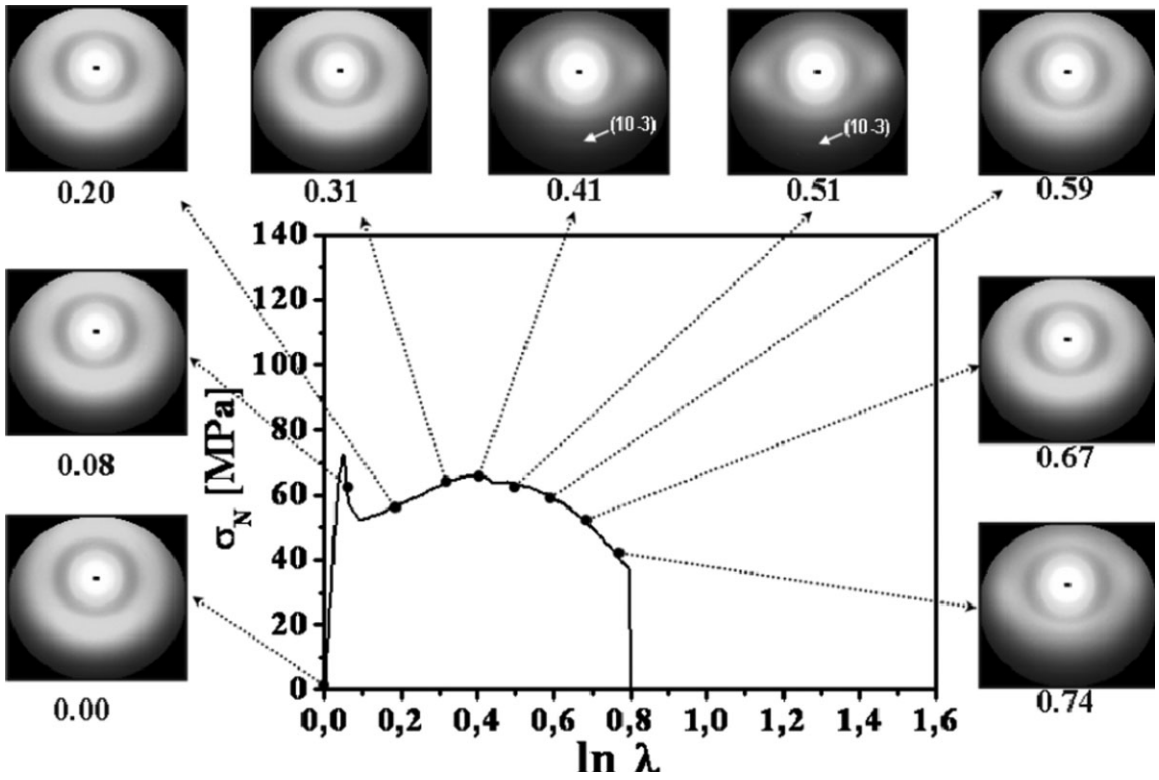

Figure 1. Homogeneous stress–strain curve and selected 2D WAXS patterns for solid state uniaxial stretching of neat PET (note: a mismatch in the WAXD patterns is observed on the neck region due to neck formation out of the incident X-ray point).

Hamburg (A2 beamline). The mechanical testing was performed on a homemade uniaxial tensile stretching device enabling to move both grips in opposed directions, so that X-ray beam is maintained at the center of the sample during the stretching procedure. Stretching apparatus output, the force and displacement curve was converted into homogeneous stress–strain curves (σ_N versus ln λ). It was assumed that the curved axisymmetric tensile specimen deforms through a rectangular neck. The stretching ratio, λ, was defined as:

$$\lambda = \frac{l}{l_0} \tag{2}$$

where l is actual tensile specimen length and l_0 the grip distance in mm. Also the homogeneous stress was calculated as follows (assuming a homogeneous deformation):

$$\sigma_N = \frac{F}{A_0}\lambda \tag{3}$$

where F is the force and A_0 the initial minimum tensile specimen cross-section area.

The specimens were mounted perpendicular to the incident X-ray beam and stretched in the vertical direction. Background scattering was subtracted and all plots were normalized with respect to the incident X-ray intensity, accumulation time, and specimen thickness (assuming a homogeneous deformation[32]). Equipmental setups were as follows:

(i) WAXS: sample-to-detector distance of 145 mm and 2D WAXS patterns were acquired with accumulation time of

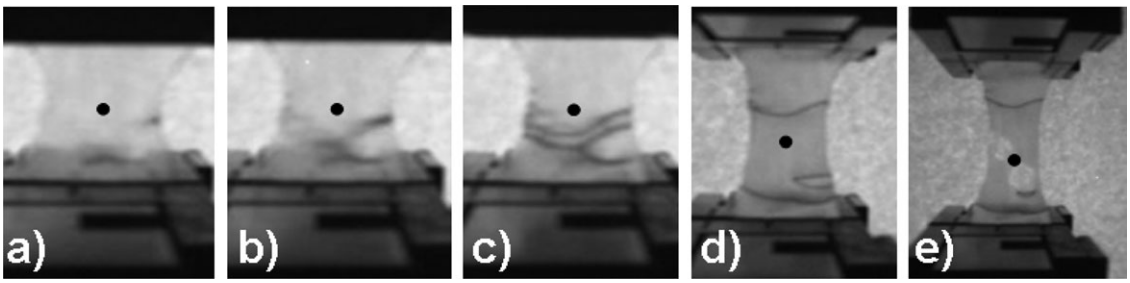

Figure 2. *In situ* video images of neat PET sample: (a) start of deformation, (b) neck initiation, (c) neck formation, (d) neck propagation, and (e) tensile bar rupture (the black spot represents approximate X-ray beam incident point).

20 s. Samples stretched at a constant crosshead velocity of 2 mmmin^{-1} (strain rate of 0.002 s^{-1}). Such accumulation time was set as a lowest as possible for considered strain rate.[33–35] WAXS was calibrated by means of a crystalline PET sample.

(ii) SAXS: sample-to-detector distance of 3025 mm and 2D SAXS patterns were acquired with accumulation time of 30 s. Samples stretched at a constant crosshead velocity of 5 mmmin^{-1} (strain rate of 0.006 s^{-1}).

Phase's Mass Fractions. The two linear intensity profiles, taken along the equatorial and meridional directions from the 2D WAXD patterns, were used to estimate mass fractions of amorphous, mesophase and periodical mesophase. A peak-fitting program was used to deconvolute the distinct phase's peaks that were fitted by a Gaussian function. The morphology of the studied samples were assumed to consist of two phases[23,36]: (i) amorphous—isotropic phase and (ii) mesophase—anisotropic phase with degree of packing and order between the crystalline and the amorphous phase. The amount of amorphous phase was assumed to be proportional to the area of the peak taken from the meridional profile. The subtraction of the amorphous fraction from the total area of the peak taken in the equatorial profile was proportional to the amount of the mesophase. The mass fractions of the individual phases were taken as the ratio of the area for each phase to the total area of the equatorial profile. As the strain increases, the WAXS patterns can exhibit a pair of meridional mesomorphic reflection $(10\bar{3})$ at about $2\Theta = 25.8°$,[37,38] indicating conformational regularity, and called periodical mesophase, PM.[39] At this stage of deformation samples morphologies were considered to be composed of three phases: (i) amorphous (ii) mesophase, and (iii) periodical mesophase—mesophase with conformational periodicity perpendicular to the stretching direction. The area of fitted $(10\bar{3})$ peak profile was used to determine the mass fraction of the PM. The sum of the area convoluted under the equatorial intensity profile and the meridional $(10\bar{3})$ peak was assumed to be the total area. The mass fractions of the individual phases were taken as the ratio of the area for each phase to the total area.

Average Polymer Orientation. The WAXS patterns were integrated along an azimuthal angle of $\mu = 0 - \pi/2$ ($\mu = 0$ at equator), over a section with width of $2\Theta = 13–28°$, to calculate the average polymer orientation, f_{av}. This sector encloses all possible crystal reflections of crystallographic planes, isotropic amorphous phase, and mesophases of PET.[40] The Hermans' orientation function was used to evaluated the average polymer orientation, $f_{av,}$ calculated as[41]:

$$f_{av} = \frac{3\langle \cos^2 \varphi \rangle - 1}{2} \tag{4}$$

where the $\langle \cos^2 \phi \rangle$ is defined as:

$$\langle \cos^2 \phi \rangle = \frac{\int_0^{\pi/2} I(\phi) \cos^2 \phi \sin \phi \, d\phi}{\int_0^{\pi/2} I(\phi) \sin \phi \, d\phi} \tag{5}$$

where ϕ is the azimuthal angle, I is the diffracted intensity and $<\cos^2\phi>$ is the average orientation function.

RESULTS AND DISCUSSION

Structural Evolution of Neat PET under Solid State Deformation

Figure 1 presents the homogeneous stress–strain curves obtained during solid state uniaxial deformation of neat PET. Selected 2D WAXS patterns are depicted along the curve (arrows indicate the strain where patterns were acquired). Video images were also collected during the stretching period (Figure 2). The stress–strain curve shows a ductile behavior of PET with a pronounced necking at low strains. WAXS patterns are showing an amorphous pattern until strain up to ln $\lambda = 0.3$, even after yielding (at strain of ln $\lambda = 0.06$). *In situ* video investigation depicted in Figure 2 shows that neck forms out of the sample center where the WAXS investigation is carried out [see Figure 2(a–c)]. As a consequence, a lack of structural evolution in the 2D WAXS patterns is observed up to this strain level. Nevertheless, the material under the X-ray beam is subjected to a load and it can be assumed as being strained before necking. During

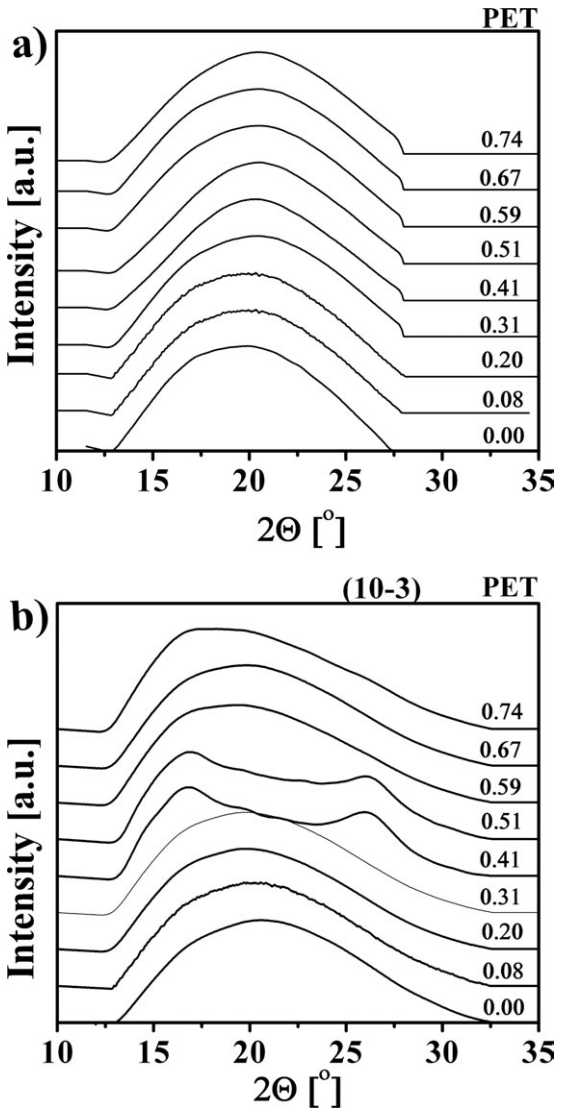

Figure 3. Linear intensity profiles extracted from 2D WAXS patterns of neat PET: (a) equatorial and (b) meridional.

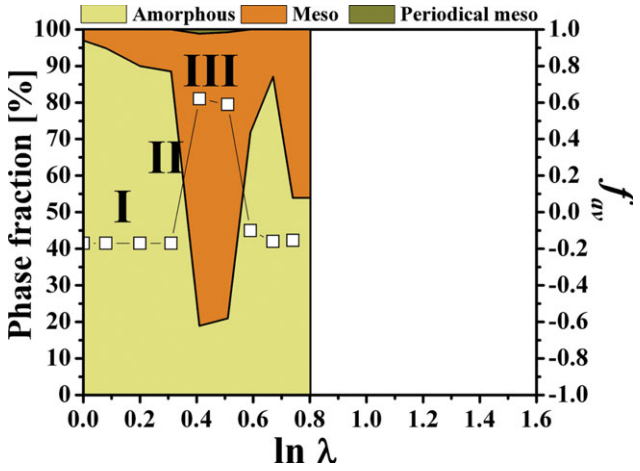

Figure 4. Neat PET phase fraction and average polymer orientation, f_{av}, evolution during solid state deformation. [Color figure can be viewed in the online issue, which is available at wileyonlinelibrary.com.]

the following interval of strain between $0.3 < \ln \lambda < 0.5$, WAXS patterns shows two diffused spots at the equator, suggesting the preferential orientation of the chains into the stretching direction.[42-47] A meridional reflection $(10\bar{3})$ can be distinguished showing the appearance of periodical mesophase.[37,38] These changes can be associated to the neck propagation through the central region of the sample as seen in Figure 2(d). At strain greater than $\ln \lambda = 0.6$ till strain of break, the stress level decreases gradually and the 2D WAXS patterns feature an amorphous hallo again. This result is suggesting local polymer chain relaxation, occurring due to macroscopic cracks appearing out of the observed zone of the tensile bar [Figure 2(e)]. Their growths lead to the specimen breakage.

The equatorial and meridional intensity profiles extracted from 2D WAXS patterns are shown in Figure 3(a, b), respectively. Initial equatorial and meridional $I - 2\theta$ profiles show an amorphous peak at about $2\theta = 20°$. Up to strains of $\ln \lambda = 0.3$, while in the equatorial profile, the same radial position is observed, the meridional diffraction shifts to a minor angle at around $2\theta = 19°$ and progresses with the appearance of the periodical mesophase $(10\bar{3})$ peak at about $2\theta = 26°$.[45,48] This plane reveals a periodical mesophase with longitudinal order, respectively a precursor formation.[42] Simultaneously, the equatorial amorphous peak narrows without a significant position change. At strain of around $\ln \lambda = 0.6$, the meridional $(10\bar{3})$ peak disappears and recovers to primary profile shape due to breakage of the sample, as explained before.

Phase's mass fraction and average polymer orientation evolution as function of strain are plotted in Figure 4. Judging by the average polymer orientation–strain curve, three main stages can be considered. Along the Stage I, the average polymer orientation remains constant as the strain increases and originally insignificant mesophase fraction undergoes a slight increment (of 8.5%). In Stage II, a rapid rise of average polymer orientation (about four times) into the stretching direction is observed, at relatively low change in strain, which causes the sharp increase of mesophase (ca. 68%) and formation of a small amount of

Table II. Characterization of the Morphologies of PET/MMT Nanocomposites

Nanocomposite	D_{av} (nm)	d (nm)	Morphology
PET/MMT32	80 ± 55	2.7	Intercalated
PET/MMT2	365 ± 300	1.9	Tactoid

D_{av}—average agglomerate diameter as calculated by eq. (1), d—interplate distance.

periodical mesophase. Between strains of $0.4 < \ln\lambda < 0.6$ Stage III takes place. Here a plateau is reached with a maximum orientation level of about 0.6 together with the highest mesophase (ca.80%) and periodical mesophase (1.5%) contents. Further stretching causes the breakage of the sample, and a sudden drop of orientation to levels almost equivalent to the Stage I is observed. Polymer chains relaxation occurs and periodical mesophase is converted into mesophase and mesophase into amorphous one.

Grounded on the above results, the structure evolution of neat PET under solid state deformation might be summarized as follows:

(1) Stage I, starts when the stretching initiates and is related to the neck initiation and formation somewhere out of the monitored central part of the tensile bar that caused no changes of average polymer orientation together with some mesophase formation. In this stage, the 2D WAXS patterns is characterized by an amorphous hallo correspondent to an equatorial $I - 2\theta$ profiles with amorphous peak at $2\theta = 20°$ while the meridional one shifts to an angle of $2\theta = 19°$.

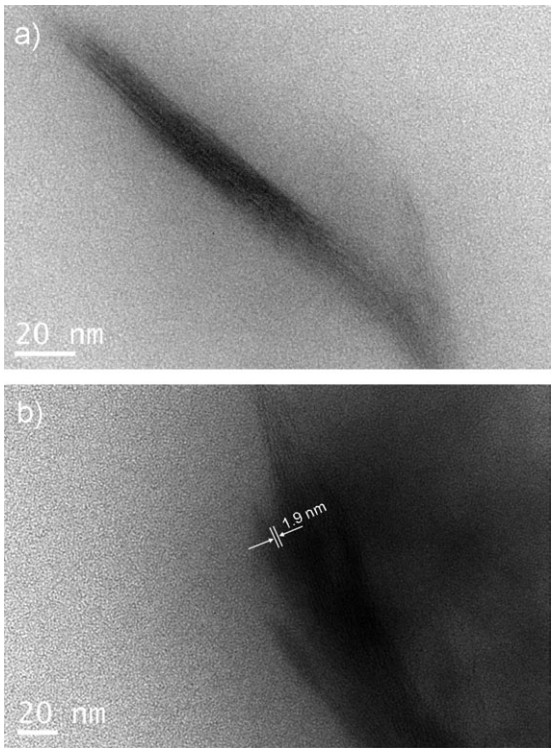

Figure 5. TEM micrographs of: (a) PET/MMT32 and (b) PET/MMT2 nanocomposites.[49]

Applied Polymer SCIENCE

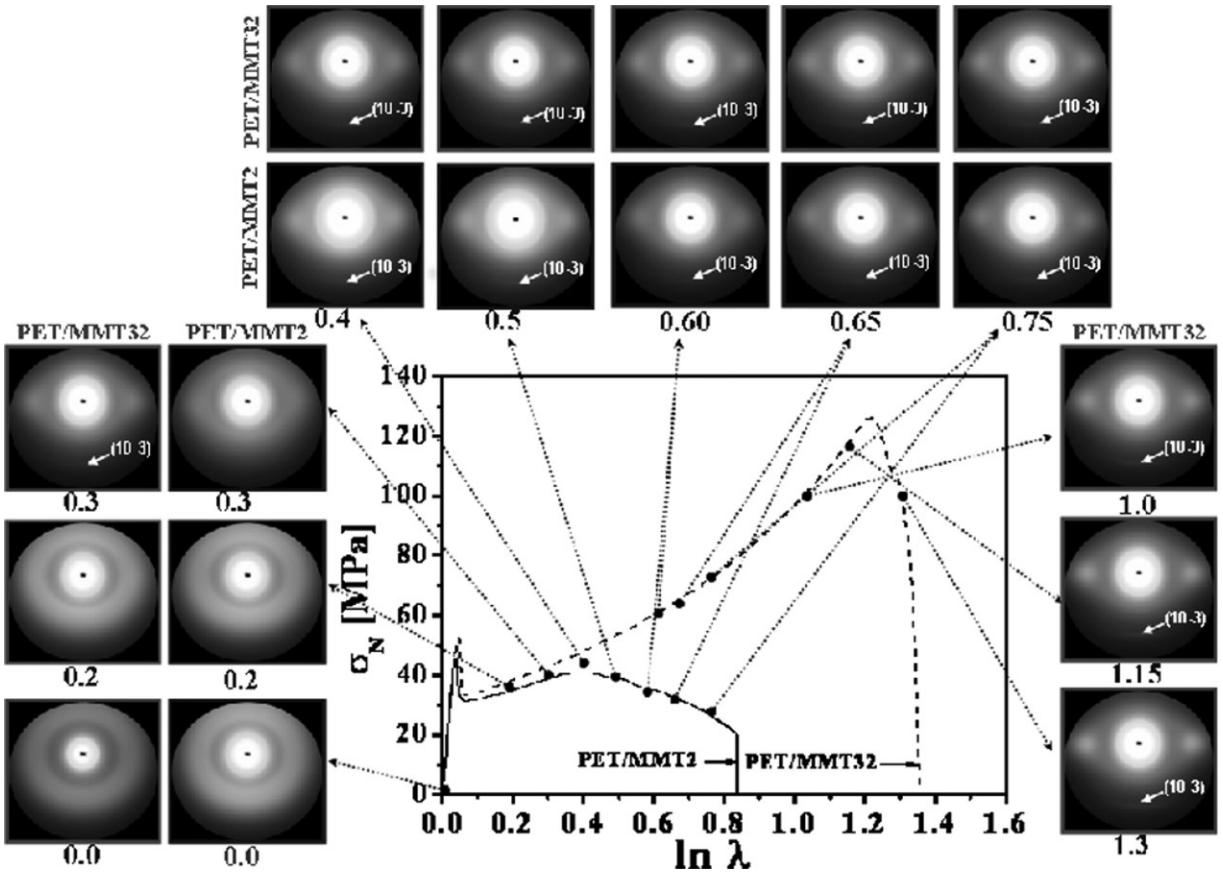

Figure 6. Homogeneous stress–strain curve and selected 2D WAXS patterns during solid state deformation of PET/MMT32 and PET/MMT2 nanocomposites. (note: a mismatch in the WAXD patterns is observed on the neck region due to neck formation out of the incident X-ray point).

(2) Further stretching leads to the beginning of Stage II that is associated to the neck propagation through the observed region of the sample (by WAXD). A sharp arise of average polymer orientation is observed together with the appearance of the meridional reflection $(10\bar{3})$, at around $2\theta = 26°$, and two spots at the equator in the 2D WAXS patterns, which translates into narrowing at same position of equatorial peak. At the same time, a tremendous amount of amorphous phase transforms into mesophase and subsequently a small of highly oriented mesophase is converted into a periodical mesophase.

(3) Stage III is representative of stable deformation through necking. As a result, the polymer chains achieve the plateau of maximum molecular orientation level. This is related to intensification of the two spots on the equator and of the $(10\bar{3})$ meridional reflection in the 2D WAXS patterns, as well as with no peaks position change in the linear intensity profile. Typical for this stage is high mesophase content and the development of periodical mesophase. In this case, at strain of $\ln \lambda = 0.6$, breakage of the tensile bar initiates via macroscopic cracks formation that results in loosing and relaxation of the molecular orientation level evidenced by an amorphous hallo in the 2D WAXS pattern. Such structural changes results into phase's relaxation, i.e., disordering of periodical mesophase into mesophase and mesophase into amorphous one.

Structural Evolution of PET/MMT under Solid State Deformation

Nanocomposites Morphology. Delamination of MMTs into the polymer matrix was observed by WAXS at low-angle range and TEM experiments. WAXS measurements did not detect any MMT basal peak (001) reflection, which could be attributed to the very low concentration of inorganic nanofillers. The dimensions of MMTs particles measured by TEM are listed in Table II. TEM results revealed comparatively homogenous dispersion of both types of MMTs. Intercalated morphology was observed in PET/MMT32 and tactoids morphology for PET/MMT2 as depicted in Figure 5 and reported elsewhere.[49]

Structure Evolution by WAXS

Homogeneous stress–strain curves and selected 2D WAXS patterns of PET/MMT nanocomposites with different morphologies, PET/MMT32—intercalated and PET/MMT2—tactoid, are depicted in Figure 6. The difference in the reinforcing nature of the intercalated and tactoid MMT's morphologies are evident, mainly, in terms of the attained stress levels, $\sigma - \ln \lambda$ curve shape, and deformation capabilities. Intercalated PET/MMT32 morphology improved the deformability and promotes higher stress levels as compare to the PET/MMT2 sample, suggesting unlike energy dissipation and deformation mechanisms, as already suggested.[28,29] When comparing to neat PET (Figure 1) only PET/MMT32 shows a considerable enhancement of the deformation capability.

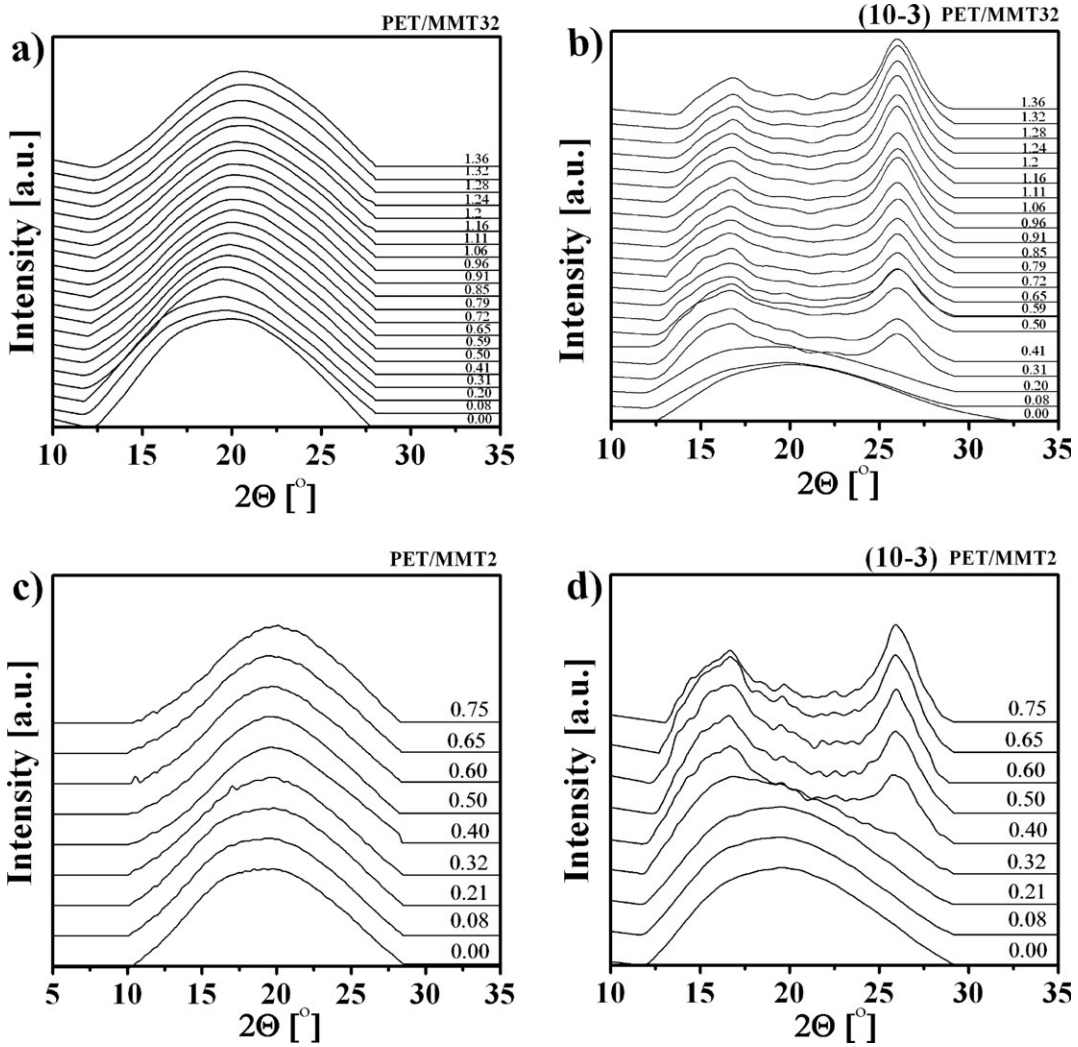

Figure 7. Linear intensity profiles extracted from 2D WAXS patterns of: PET/MMT32 nanocomposite (a) equatorial and (b) meridional and PET/MMT2 nanocomposite: (c) equatorial and (d) meridional.

Regardless of their morphology, both nanocomposites exhibit identical neck evolution to neat PET. Hence both nanocomposites feature amorphous 2D WAXS patterns, during the first part of $\sigma_N - \ln \lambda$ curve, similar to those of pure PET. This corresponds to a lack of structural evolution as detected by WAXS, originated by delay of the neck propagation thought incident X-ray point on

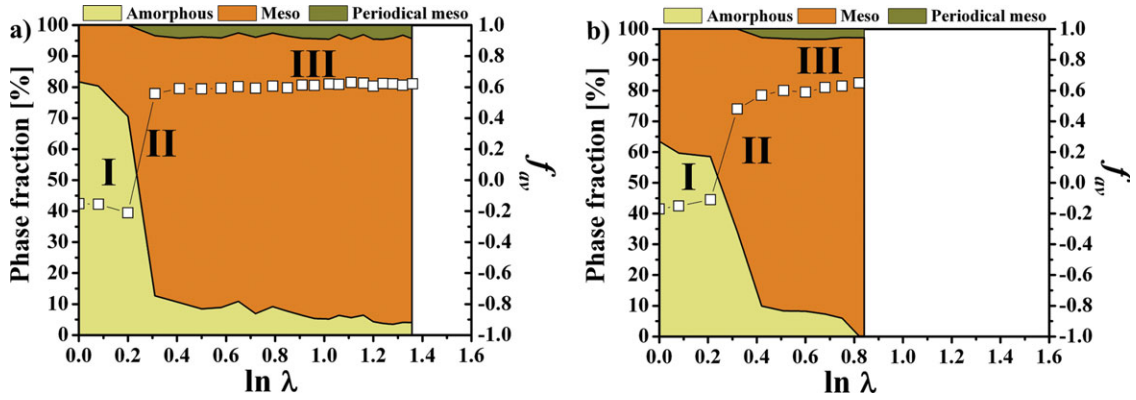

Figure 8. Phase fraction and average polymer orientation, $f_{av,}$ evolution of: (a) PET/MMT32 and (b) PET/MMT2 nanocomposites. [Color figure can be viewed in the online issue, which is available at wileyonlinelibrary.com.]

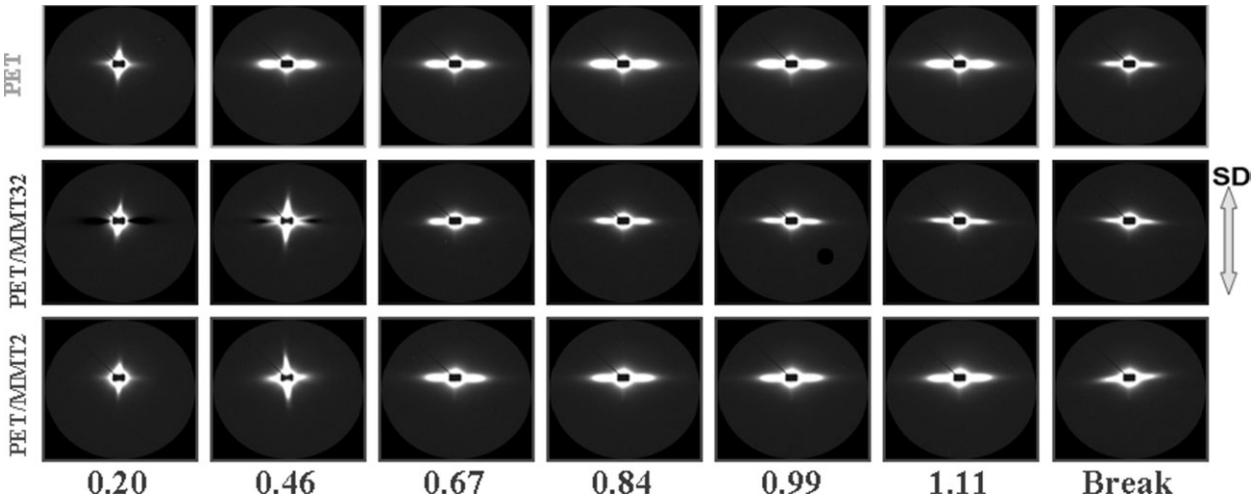

Figure 9. Selected 2D SAXS patterns and corresponding strain, lnλ, obtained during the *in situ* SAXS characterization.

the tensile bar. In 2D WAXS patterns of nanocomposites, when neck propagates through observed region, the periodical mesophase reflection $(10\bar{3})$ at meridian and two spots on the equator appears at dissimilar strain level, i.e., ln$\lambda = 0.3$ in case of PET/MMT32 and at ln$\lambda = 0.4$ for PET/MMT2.

Figure 7 shows the equatorial and meridional intensity profiles extracted from the 2D WAXS patterns of both PET/MMT nanocomposites. In the equatorial intensity profiles before stretching are observed the amorphous peaks at about $2\theta = 20°$, which intensify with stretching till different strain levels, namely for PET/MMT32 up to ln $\lambda = 0.3$ and PET/MMT2 to ln $\lambda = 0.4$, respectively. From these strain further, they intensify with stretching and shift to angle $\sim 2\theta = 21°$, [Figure 7(a, c)]. On the other hand, the amorphous peaks in the meridional $I - 2\theta$ profiles, during a low strain interval, i.e., $0 <$ ln $\lambda < 0.3$ for PET/MMT32 and $0 <$ ln $\lambda < 0.4$ for PET/MMT2, intensify and shift from $2\theta = 20°$ to $2\theta = 19°$. Thereafter, at about $2\theta = 26°$ the periodical mesophase peak reflection $(10\bar{3})$ appears. As in the neat PET, a periodical mesophase is formed. This peak intensity increases with stretching [Figure 7(b, d)] indicating a better perfection of the precursor structure.

Nanocomposites phases and average polymer orientation evolutions with deformation are depicted in Figure 8(a) for PET/MMT32 and in Figure 8(b) for PET/MMT2 samples. Based on the similar shapes of the average polymer orientation vs. ln λ curve, of both nanocomposites, it might be defined three main stages as designated in Figure 8: (i) during Stage I, there is no variation of polymer orientation while moderate amount of amorphous phase organizes into mesophase. (ii) In Stage II, there is a sharp increment of average orientation assisted by a rapid mesophase increase at the expenses of amorphous phase consumption and a little portion of mesophase orders into periodical mesophase. (iii) Finally, in Stage III, the samples reach a plateau of maximum orientation level and also a maximum periodical mesophase content that remain almost without alterations along this stage. The mesophase fraction slightly increases during stretching.

Initially, as-molded PET/MMT2 nanocomposite sample has almost the double amount of mesophase than the PET/MMT32 one (with 18%). Intercalated PET/MMT32 sample shown anticipate formation of periodical mesophase, at strain of ln$\lambda =$ 0.3, than the tactoid PET/MMT2 one (ln$\lambda = 0.4$). Along Stage III, the nanocomposites are characterized by similar maximum average orientation level (of around $f_{av} = 0.6$) and slightly different of periodical mesophase fraction, i.e., about 4% for PET/MMT32 and about 3% for PET/MMT2.

With respect to the PET sample, the nanocomposites, apart from their distinct morphology, attained during the Stage III a similar maximum orientation level and a higher amount of mesophase and consequently of periodical mesophase. On the other hand, intercalated morphology of PET/MMT32 nanocomposite caused an earlier formation of periodical mesophase than neat PET.

The general structure evolution of the PET/MMT nanocomposites, assessed by the WAXS investigations can be summarized as follows:

1. Stages I, embraces the low strain levels of mechanical response, before neck forms causing no alterations neither of polymer orientation and nor of amorphous hallo in the 2D WAXS pattern, but a slight intensification in both $I - 2\theta$ profiles and shift to $2\theta = 19°$, associated to the transformation of some amorphous phase into mesophase.
2. Start of Stage II is marked by sharp increase of average polymer orientation, cause by necking, being translated into the appearance of two equatorial spots and a meridional $(10\bar{3})$ reflection in the 2D WAXS patterns. Such rapid increase of polymer chains orientation leads to fast formation of a high fraction of mesophase at expansion of the amorphous phase and the nucleation of a periodical mesophase as a result of the high mesophase orientation.

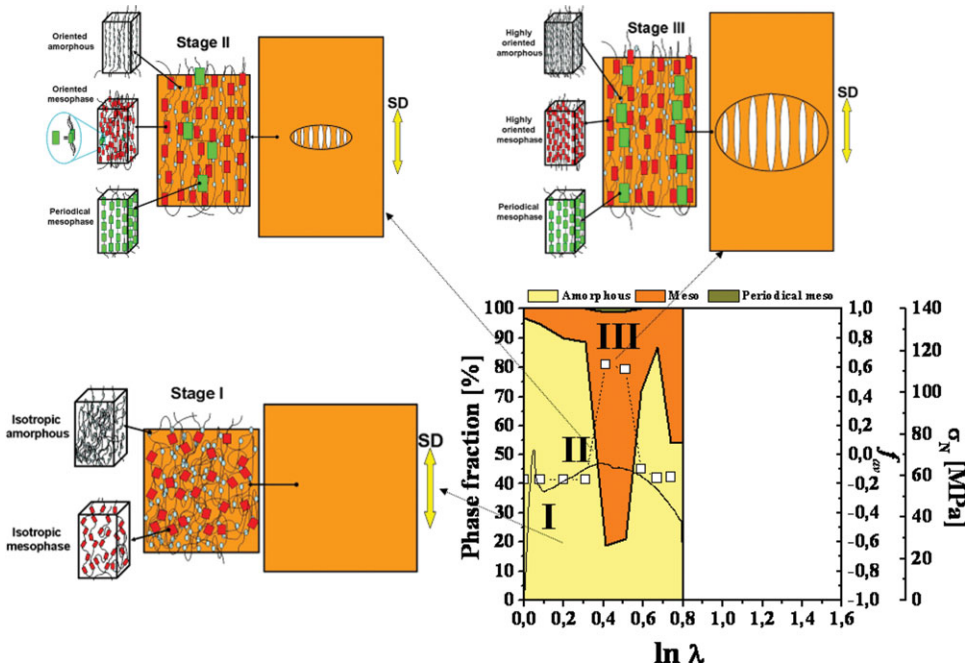

Figure 10. Schematic diagram illustrating the multiscale structure evolution during in solid state uniaxial stretching of neat PET (note: a mismatch in the WAXD patterns is observed on the neck region due to neck formation out of the incident X-ray point). [Color figure can be viewed in the online issue, which is available at wileyonlinelibrary.com.]

3. The stable deformation through necking corresponds to the Stage III, where the polymer orientation levels off at a maximum level of around 0.6. WAXS equatorial spots intensify and shift peak to $2\theta = 21°$, whereas $(10\bar{3})$ reflection shows amplification at about $2\theta = 26°$. The periodical mesophase content remains almost intact and the mesophase fraction slightly increase till sample rupture.

Structure Evolution by SAXS

Figure 9 shows selected 2D SAXS patterns of neat PET and its MMT nanocomposites obtained along the plastic deformation region of the $\sigma_N - \ln\lambda$ curve. Based on the characteristic features occurring in 2D SAXS patterns during stretching it can be denoted distinct differences in the structure evolution of nanocomposites, due to dissimilar deformation mechanisms taking place. These are dependent on the specimen morphology.

All samples show in the first patterns a streak parallel to the stretching direction, at $\ln\lambda = 0.2$, which is originated by crazes within polymer matrix at craze/polymer interfaces.[50] Crazes are typical for amorphous polymer during solid state deformation, as reported for neat PET[51–53] and for its nanocomposites.[30,31] With further stretching, at strain of $\ln\lambda = 0.46$, the 2D SAXS patterns show different shapes: the streak perpendicular to the loading direction, in the case of neat PET is caused by the fibril/void elongation in the stretching direction.[50,54] The cross-shaped pattern observed for both MMT nanocomposites, represents in the meridional streak the reflection crazes formed at the craze/polymer interfaces[50,54] and in the equatorial the fibril/void structure of crazes and some voids formed inside the MMT particles and tactoids, respectively.[28,29]

These dissimilar pattern shapes at identical strain level can be related to retarded growth of the crazes in the polymer bulk, as compared to the neat PET, due to MMT's incorporation, as already reported elsewhere.[30,31] Further stretching, greater than $\ln\lambda = 0.7$, leads to the transformation of 2D SAXS patterns of all investigated samples into equatorial streaks associated to elongation of voids parallel to the stretching direction.[54] Those might be caused by the elongated voids inside the crazes within polymer matrix and by voids between the MMTs particles.[55]

On the other hand, by the equatorial streaks height it may be estimated the void's height and from its length their diameter.[50,54] Qualitative analyses of the dimensions of the equatorial streaks, at strains greater than $\ln\lambda = 0.7$ till samples breakage, suggest that voids in the neat PET sample have a slightly bigger height and diameter to those in the PET/MMT2 nanocomposites. The PET/MMT32 nanocomposite seems to develop the voids with the smallest height and diameter of all studied samples. Among the PET/MMT nanocomposites tactoid morphology of PET/MMT2 nanocomposite induces a bigger size voids than the intercalated PET/MMT32 one, in accordance with previous observations.[28,29]

MULTISCALE STRUCTURAL EVOLUTION MODELS

Strain-induced structure transitions and deformation mechanism upon uniaxial stretching in solid state of PET and its MMT nanocomposites can be interpreted by the multiscale models depicted in Figure 10.

Applied Polymer SCIENCE

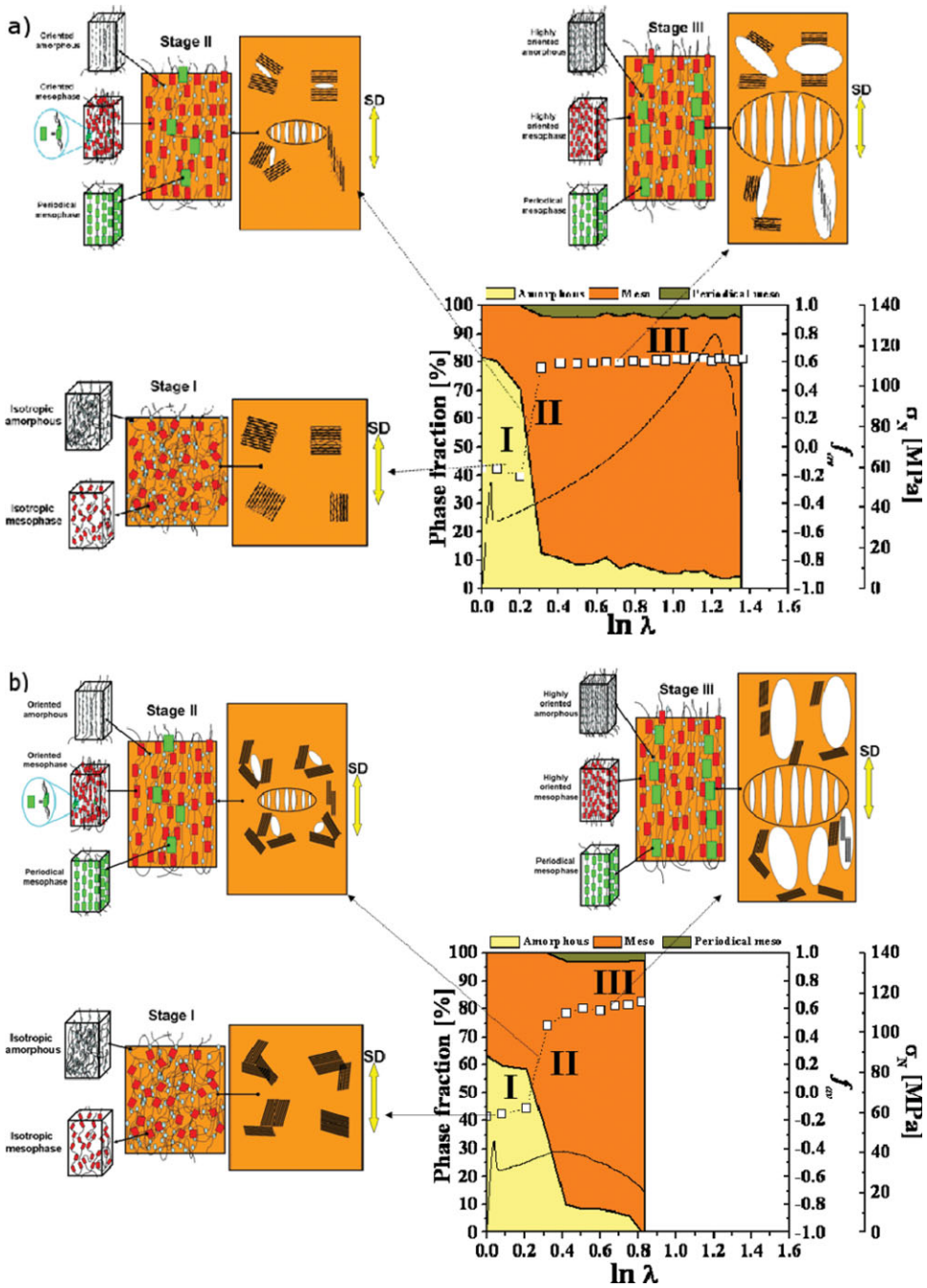

Figure 11. Schematic diagram illustrating the multiscale structure evolution during solid state uniaxial stretching of (a) intercalated and (b) tactoid in PET/MMT nanocomposites (note: a mismatch in the WAXD patterns is observed on the neck region due to neck formation out of the incident X-ray point). [Color figure can be viewed in the online issue, which is available at wileyonlinelibrary.com.]

The multiscale structure evolution of neat PET can be explained as follows (Figure 9):

1. Stage I: It is descriptive for the structure evolution at initial strain levels before necking occurs (recall that neck formed along the tensile bar out of observed region). A small amount of initial isotropic amorphous phase transforms into mesophase, at constant average polymer orientation.
2. Stage II: is the shortest stage correspondent to the neck formation under X-ray beam: crazes are formed and widen perpendicular to the stretching direction. The polymer chains achieve the maximum orientation level causing a rapid transformation of oriented amorphous phase into mesophase and promoting the appearance of periodical mesophase originated by the orientation of the mesophase.

3. Stage III: is related to the tensile bar lengthening through necking. The maximum average polymer orientation level is achieved and remains constant throughout, corresponding to the polymer chains extensibility limits resulting into maximum content of highly oriented mesophase and periodical mesophase. Simultaneously voids and crazes extend into the stretching direction. At ultimate strain levels rupture of the sample occurs. Fail of fibrils within crazes originates microvoids enlargement till sample collapses. In this case, microvoids evolve into macrocracks [57] causing a local relaxation of polymer orientation, and periodical mesophase is transformed into mesophase and mesophase into amorphous phase.

Generally, the evolution of both nanocomposite morphologies, i.e., tactoid and intercalated, have quite similar pathways. The main difference is the bigger size of voids caused by the deformation of the MMTs tactoids.[28] The description of multiscale model of strain-induced structure evolution of intercalated and tactoid PET/MMT nanocomposites during the stretching in solid state are shown respectively in Figure 11(a, b). The main stages can be described as follows:

1. Stage I: it is characterized by a negligible or very small evolution of the average polymer orientation, with a slight development of mesophase from isotropic amorphous one. This stage is valid from the start of stretching until neck reaches the observed part of the sample.
2. Stage II: As the neck progresses over the observed region, a fast increase of the average polymer orientation in the stretching direction is observed that leads to the development of high amount of mesophase from the amorphous phase and to the formation of a periodical mesophase. Simultaneously, polymer crazes appear and the MMT's intercalated particles/tactoids break, creating voids inside the intercalated MMT/tactoids.[28,29] Further deformation takes place also within the intercalated MMT's particles/tactoids. Several mechanisms can occur, either opening when intercalate particles/tactoids are perpendicular to the stretching direction; opening of particles/bundles occurring when the intercalate particles/tactoids are oriented at certain angle to the stretching direction; or platelets slipping/bundles when intercalated particles/tactoids are parallel to the stretching direction.[28,29] However, the crazes-like structures widening within the polymer matrix is hampered by MMTs.[30]
3.. Stage III: it is characterized by a plateau of the average polymer orientation and maintenance of the mesophase and periodical mesophase. Macroscopically it corresponds to the deformation through stable necking. Voids within crazes and those originated by the MMTs intercalated particles/tactoids advance into microvoids due to platelets/bundles displacement that lead to elongation in the stretching direction. Finally it results in sample breakage. With further deformation, a slow transformation of oriented amorphous into mesophase occurs. The tensile bar rupture is a result of merge of microvoids.

CONCLUSIONS

The evolution of strain-induced phase transition and average polymer orientation with strain increment was investigated for neat PET and its nanocomposites with MMT with distinct initial morphologies: tactoids and intercalated MMT particles. Both MMT morphologies show distinct structure evolution during stretching. Distinct structural models were proposed for each type of initial MMT nanocomposite morphology and neat PET, interpreting the obtained experimental results. PET and its nanocomposites multiscale structure evolution have three main common stages:

i. Stage I (before necking): a small amount of amorphous phase evolves into mesophase at constant molecular orientation level;
ii. Stage II (at necking): a rapidly increase of polymer molecular orientation originates a sharp increment of mesophase at the expenses of the amorphous phase and the formation of a periodical mesophase from the mesophase. Also craze-like structures are formed and widen in the polymer bulk and, in case of nanocomposites, voids also appear inside the MMTs particles; and
iii. Stage III (neck propagation): at leveling off of the average molecular orientation, the highest periodical mesophase content is achieved, as well as a slight increment of mesophase upon further deformation. Along this stage, crazes within polymer matrix and voids from the MMTs layers separation evolve into microvoids.

Intercalated PET/MMT32 exposed considerable enhancement of attained stress level and deformation capability of polymer matrix in comparison to the neat PET, while the tactoid structure of PET/MMT2 causes only slight improvements. All investigated samples, regardless of their morphologies, reached similar maximum orientation level. Incorporating MMT nanofillers in PET matrix promoted a higher fraction of mesophase and, at elevated strains, of periodical mesophase as compared to neat PET. MMT intercalation in the case of PET/MMT32 causes an earlier formation and enhanced amount of periodical mesophase than the tactoid PET/MMT2 and neat PET. Crazes appear within the PET matrix in all samples, at earlier stages of plastic deformation. Both nanocomposites morphologies retarded crazes widen within the polymer bulk. Intercalated morphology PET/MMT32 leads to formation of voids with the smallest height and diameter in between the considered specimens. Tactoid PET/MMT2 sample results into voids with dimensions alike to the pure PET.

ACKNOWLEDGMENTS

The authors thank Süd-Chemie AG, Germany for donating the nanoparticles. This work was financially supported by: (i) DESY and the European Commission under: a) HASYLAB Project DESY-D-II-05-101 EC, and b) the FP6 contracts RII3-CT-2004-506008 (IA-SFS); (ii) the Portuguese Foundation for Science and Technology, FCT, through: a) project POCI/V.5/A0094/2005 (ADFUN_PACK), and b) PhD student grant SFRH/BD/44917/2008.

REFERENCES

1. Koo, J. H. Polymer Nanocomposites Processing, Characterization, and Applications; McGraw-Hill: New York, **2006.**
2. Shah, D.; Maiti, P.; Gunn, E.; Schmidt, D. F.; Jiang, D. D.; Batt, C. A.; Giannelis, E. P. *Adv. Mater.* **2004,** *16*, 1173.
3. Dennis, H. R.; Hunter, D. L.; Chang, D.; Kim, S.; White, J. L.; Cho, J. W.; Paul, D. R. *Polymer* **2001,** *42*, 9513.
4. Jordan, J.; Jacob, K. I.; Tannenbaum, R.; Sharaf, M. A.; Jasiuk, I. *Mater. Sci. Eng. A* **2005,** *393*, 1.
5. Paul, D. R.; Robeson, L. M. *Polymer* **2008,** *49*, 3187.
6. Tjong, S. C. *Mater. Sci. Eng. R Rep.* **2006,** *53*, 73.
7. Liu, J.; Boo, W. J.; Clearfield, A.; Sue, H. J. *Mater. Manufact. Process.* **2006,** *21*, 143.
8. Ray, S. S.; Okamoto, M. *Progr. Polym. Sci. (Oxford)* **2003,** *28*, 1539.
9. Ou, C. F.; Ho, M. T.; Lin, J. R. *J. Appl. Polym. Sci.* **2004,** *91*, 140.
10. Barber, G. D.; Moore, R. B. *ACS PMSE Proc.* **2000,** *82*, 241.
11. Ou, C. F.; Ho, M. T.; Lin, J. R. *J. Polym. Res.* **2003,** *10*, 127.
12. Sanchez-Solis, A.; Garcia-Rejon, A.; Manero, O. *Macromol. Symp.* **2003,** *192*, 281.
13. Davis, H. R.; Mathias, L. J.; Gilman, J. W.; David, A.; Schiraldi, J.; Shields, R.; Trulove, T.; Sutto, T. E.; Delong, C. H. *J. Polym. Sci. B Polym. Phys.* **2002,** *40*, 2661.
14. Wang, Y.; Gao, J.; Ma, Y.; Agarwal, U. S. *Compos. B Eng.* **2006,** *37*, 399.
15. Barber, G. D.; Calhoun, B. H.; Moore, R. B. *Polymer* **2005,** *46*, 6706.
16. Sanchez-Solis, A.; Romero-Ibarra, I.; Estrada, M. R.; Calderas, F.; Manero, O. *Polym. Eng. Sci.* **2004,** *44*, 1094.
17. Pegoretti, A.; Kolarik, J.; Peroni, C.; Migliaresi, C. *Polymer* **2004,** *45*, 2751.
18. Bizarria, M. T. M.; Giraldi, A. L. F. M.; Carvalho, C. M.; Velasco, J. I.; d'Ávila, M. A.; Mei, L. H. I. *J. Appl. Polym. Sci.* **2007,** *104*, 1839.
19. Kracalik, M.; Studenovsky, M.; Mikesova, J.; Kovarova, J.; Sikora, A.; Thomann, R.; Friedrich, C. *J. Appl. Polym. Sci.* **2007,** *106*, 2092.
20. Kracalik, M.; Mikesova, J.; Puffr, R.; Baldrian, J.; Thomann, R.; Friedrich, C. *Polym. Bull.* **2007,** *58*, 313.
21. Chung, J. W.; Son, S.-B.; Chun, S.-W.; Kang, T. J.; Kwak, S.-Y. *Polym. Degrad. Stabil.* **2008,** *93*, 252.
22. Sanchez-Solis, A.; Garcia-Rejon, A.; Estrada, M.; Martinez-Richa, A.; Sanchez, G.; Manero, O. *Polym. Int.* **2005,** *54*, 1669.
23. Todorov, L. V.; Viana, J. C. *J. Appl. Polym. Sci.* **2007,** *106*, 1659.
24. Bizarria, M. T. M.; Giraldi, A. L. F. M.; Carvalho, C. M.; Velasco, J. I.; d'Ávila, M. A.; Mei, L. H. I. Morphology and thermomechanical properties of recycled PET-organoclay nanocomposites. *J. Appl. Polym. Sci.* **2007,** *104*, 1839.
25. Alyamac, E.; Yilmazer, U. *Polym. Compos.* **2007,** *28*, 251.
26. Kracalik, M.; Mikesova, J.; Puffr, R.; Baldrian, J.; Thomann, R.; Friedrich, C. *Polym. Bull.* **2007,** *58*, 313.
27. Kracalik, M.; Studenovsky, M.; Mikesova, J.; Kovarova, J.; Sikora, A.; Thomann, R.; Friedrich, C. *J. Appl. Polym. Sci.* **2007,** *106*, 2092.
28. Kim, G. M.; Lee, D. H.; Hoffmann, B.; Kressler, J.; Stöppelmann, G. *Polymer* **2001,** *42*, 1095.
29. Kim, G. M.; Goerlitz, S.; Michler, G. H. *J. Appl. Polym. Sci.* **2007,** *105*, 38.
30. Kobayashi, H.; Shioya, M.; Tanaka, T.; Irisawa, T. *Compos. Sci. Technol.* **2007,** *67*, 3209.
31. Kobayashi, H.; Shioya, M.; Tanaka, T.; Irisawa, T.; Sakurai, S.; Yamamoto, K. *J. Appl. Polym. Sci.* **2007,** *106*, 152.
32. Oultache, A. K.; Kong, X.; Pellerin, C.; Brisson, J.; Pezolet, M.; Prud'homme, R. E. *Polymer* **2001,** *42*, 9051.
33. Todorov, L. V.; Viana, J. C. *Int. J. Mater. Forming* **2008,** *1*, 661.
34. Todorov, L. V.; Martins, C. I.; Viana, J. C. *J. Appl. Polym. Sci.* **2012,** *124*, 470.
35. Todorov, L. V. Institute for Polymers and Composites/I3N; Department of Polymer Engineering University of Minho: Guimarães, **2011.**
36. Todorov, L. V.; Martins, C. I.; Viana, J. C. *J. Appl. Polym. Sci.* **2011,** *120*, 1253.
37. Parravicini, L.; Leone, B.; Auriemma, F.; Guerra, G.; Petraccone, V.; Dino, G. D.; Bianchi, R.; Vosa, R. *J. Appl. Polym. Sci.* **1994,** *52*, 875.
38. Goschel, U. *Polymer* **1996,** *37*, 4049.
39. Todorov, L. V.; Martins, C. I.; Viana, J. C. Solid-state structural evolution of poly(ethylene terephthalate) during step uniaxial stretching from different initial morphologies: An in situ wide angle x-ray scattering study. J. Appl. Polym. Sci. **2011.** *124*, 470.
40. Goschel, U.; Deutschert, K.; Abetzt, V. *Polymer* **1996,** *37*, 1.
41. Stribeck, N. X-ray Scattering of Soft Matter; Springer: Berlin, **2007.**
42. Ran, S.; Wang, Z.; Burger, C.; Chu, B.; Hsiao, B. S. Mesophase as the Precursor for Strain-Induced Crystallization in Amorphous Poly(ethylene terephthalate) Film. *Macromolecules* **2002,** *35*, p. 10102–10107.
43. Blundell, D. J.; MacKerron, D. H.; Fuller, W.; Mahendrasingam, A.; Martin, C.; Oldman, R. J.; Rule, R. J.; Riekel, C. *Polymer* **1996,** *37*, 3303.
44. Kawakami, D.; Ran, S.; Burger, C.; Fu, B.; Sics, I.; Chu, B.; Hsiao, S. B. Mechanism of Structural Formation by Uniaxial Deformation in Amorphous Poly(ethylene terephthalate) above the Glass Temperature. *Macromolecules* **2003,** *3*, p 9275–9280.
45. Kawakami, D.; Hsiao, B. S.; Ran, S.; Burger, C.; Fu, B.; Sics, I.; Chu, B.; Kikutani, T. *Polymer* **2004,** *3*, 905.
46. Kawakami, D.; Ran, S.; Burger, C.; Avila-Orta, C.; Sics, I.; Chu, B.; Benjamin, S. H.; Kikutani, T. *Macromolecules* **2006,** *39*, 2909.
47. Martins, C. I.; Cakmak, M. *Polymer* **2007,** *48*, 2109.
48. Kawakami, D.; Ran, S.; Burger, C.; Fu, B.; Sics, I.; Chu, B.; Hsiao, S. B. *Macromolecules* **2003,** *36*, 9275.

49. Todorov, L. V.; Martins, C. I.; Viana, J. C. *Solid State Phenomena* **2009,** *151*, 113.

50. Shioya, M.; Kawazoe, T.; Okazaki, R.; Suei, T.; Sakurai, S.; Yamamoto, K.; Kikutani, T. *Macromolecules* **2008,** *41*, 4758.

51. Liu, Y.; Kennard, C. H. L.; Truss, R. W.; Calos, N. J. *Polymer* **1997,** *38*, 2797.

52. Viana, J. C.; Mano, J. F.; Denchev, Z. Z.; Oliveira, M. J.; Cramez, M. C. Nanostructure Evolution during Uni-axial Deformation of PET a WAXS and SAXS Study using Synchrotron Radiation *Mater. Sci. Forum* **2006,** p. 1583–1587.

53. Efimov, A. V.; Shcherba, V. Y.; Bakeyev, N. F. *Polym. Sci. USSR* **1991** *33*, 568.

54. Stribeck, N.; Nochel, U.; Fakirov, S.; Feldkamp, J.; Schroer, C.; Timmann, A.; Kuhlmann, M., *Macromolecules* **2008,** *41*, 7637.

55. Ren, C.; Jiang, Z.; Du, X.; Men, Y.; Tang, T. *J. Phys. Chem. B* **2009,** *113*, 14118.